Superhydrophilicity of a nanofiber-covered aluminum surface fabricated via pyrophosphoric acid anodizing

Daiki Nakajima, Tatsuya Kikuchi*, Shungo Natsui, and Ryosuke O. Suzuki
Faculty of Engineering, Hokkaido University
N13-W8, Kita-ku, Sapporo, Hokkaido, 060-8628, Japan

*Corresponding author: Tatsuya Kikuchi
TEL: +81-11-706-6340
FAX: +81-11-706-6342
E-mail: kiku@eng.hokudai.ac.jp

Highlights

Superhydrophilicity of a nanofiber-covered aluminum surface was investigated.

Anodic alumina nanofibers were formed via pyrophosphoric acid anodizing.

Nanofiber-covered aluminum surface displays fast and stable superhydrophilicity.

The quick-drying and snow-sliding behaviors were demonstrated.

Abstract

A superhydrophilic aluminum surface covered by numerous alumina nanofibers was fabricated via pyrophosphoric acid anodizing. High-density anodic alumina nanofibers grow on the bottom of a honeycomb oxide via anodizing in concentrated pyrophosphoric acid. The water contact angle on the nanofiber-covered aluminum surface decreased with time after a 4-μL droplet was placed on the surface, and a superhydrophilic behavior with a contact angle measuring 2.2° was observed within 2 s; this contact angle is considerably lower than those observed for electropolished and porous alumina-covered aluminum surfaces. There was no dependence of the superhydrophilicity on the density of alumina nanofibers fabricated via different constant voltage anodizing conditions. The superhydrophilic property of the surface covered by anodic alumina nanofibers was maintained during an exposure test for 359 h. The quick-drying and snow-sliding behaviors of the superhydrophilic aluminum covered with anodic alumina nanofibers were demonstrated.

Keywords: Aluminum; Anodizing; Anodic Alumina Nanofibers; Pyrophosphoric Acid; Superhydrophilicity

1. Introduction

Aluminum anodizing is a simple electrochemical technique that is used to form thick anodic oxide films on an aluminum surface and has been widely investigated in the fields of surface science and engineering for corrosion protection, electronic devices, and optical materials [1-7]. Anodic oxide films fabricated via aluminum anodizing can be typically classified into the following two groups: barrier type oxide films formed in neutral solutions and porous type oxide films (porous alumina) formed in acidic and alkaline solutions [1,2,8-18]. Typically, anodizing in acidic solutions, such as sulfuric (H_2SO_4), oxalic ($(COOH)_2$), and phosphoric acid (H_3PO_4), causes the formation of porous alumina which consists of numerous nanoscale hexagonal cells measuring several tens or hundreds of nanometers in diameter with a nanopore at the center of each cell [19-25]. There has been interest in the characteristic nanostructure of porous alumina for their chemical and physical properties [26-30].

Recently, the fabrication of third-generation anodic oxide, anodic alumina nanofibers, which are different from the nanofeatures of barrier and porous oxides, has been reported by several research groups [31-34]. The fabrication processes for the alumina nanofibers are based on the typical anodizing in acidic solutions for the formation of porous alumina and the subsequent selective chemical etching of the porous alumina. High-aspect-ratio alumina nanofibers that are several tens or hundreds of nanometers in diameter can be fabricated via these processes, and the aluminum surface that is covered by the alumina nanofibers exhibits unique hydrophilic and hydrophobic behaviors. However, the fabrication of alumina nanofibers is based on multiple steps including long-term anodizing and chemical etching. In addition, the nanostructural features of alumina nanofibers, including their length, density, and uniformity, could not be controlled accurately in the previous investigations. Therefore, the development of a simple and rapid anodizing process is required for the formation of anodic alumina nanofibers on an aluminum substrate.

We have demonstrated the fabrication of anodic alumina nanofibers via a simple anodizing technique in a new electrolyte, pyrophosphoric acid ($H_4P_2O_7$) [35]. Pyrophosphoric acid anodizing readily creates ultra-high density ($10^{10}/cm^2$) alumina nanofibers with single nanometer-scale diameters [36]. Structural control of the alumina nanofibers, such as the length and density, can be achieved by an electrochemical approach during the anodizing. Well-defined, high-density, and highly ordered alumina nanofibers with a 37-75 nm periodic spacing have successfully been fabricated via novel two distinct anodizing processes [37]. In these investigations to characterize the alumina nanofibers, we found that an aluminum surface covered by high-density alumina fibers exhibited ultra-fast superhydrophilic behavior with a contact angle near zero within 1 s after the distilled water drop was placed on the surface [35]. Because this novel aluminum surface covered by numerous alumina nanofibers is of great interest for various surface science and engineering endeavors, the superhydrophilic behavior of the aluminum surface should be further investigated.

In the present investigation, we studied the superhydrophilicity of the nanofiber-covered aluminum surface fabricated via pyrophosphoric acid anodizing. The effect of surface nanofeatures on the hydrophilic behavior was determined by microscopy observations and wettability measurements, and the applications of this surface for quick-drying and snow-sliding materials were demonstrated.

2. Experimental

High purity aluminum plates (99.99 wt%, 20 mm × 40 mm, 400 μm thick, Nippon Light Metal, Japan) were used as the starting materials. The aluminum specimens were ultrasonically degreased in ethanol for 10 min and then were electropolished in a 13.6 M CH_3COOH/ 2.56 M $HClO_4$ mixture (78 vol% CH_3COOH/22 vol% 70% $HClO_4$, T = 280 K) at a constant voltage of 28 V for 1 min. A large aluminum plate was used as the cathode for electropolishing.

The electropolished specimens were immersed in a concentrated pyrophosphoric acid solution (74.0-78.0 wt%, T = 293 K, Kanto Chemical, Japan) and were anodized at constant cell voltages of U = 25-75 V for up to t_a = 60 min. A high purity platinum plate was used as the cathode for anodizing, and the pyrophosphoric acid solution was slowly stirred with a magnetic stirrer during anodizing. A constant voltage was applied to the electrodes using a direct current power supply (PWR-400H, Kikusui, Japan) connected to a PC. The current density was monitored by a digital multimeter (DMM4040, Tektronix) during the constant voltage anodizing. The electrolyte solutions were maintained at a constant temperature using a water bath (UCT-1000, AS ONE, Japan). After anodizing, the specimens were immediately removed from the pyrophosphoric acid solution and then washed with distilled water and dried in a desiccator. For a comparison of the hydrophilic behaviors, the electropolished aluminum specimens were also anodized under the typical anodizing conditions for the formation of several types of porous alumina, in a) a 0.5 M sulfuric acid at 25 V and 283 K, b) a 0.3 M oxalic acid at 50 V and 293 K, and c) a 0.3 M phosphoric acid at 160 V and 273 K.

The nanomorphology of the anodized specimens was examined by field emission scanning electron microscopy (FE-SEM, JIB-4600F/HKD and JSM-6500F, JEOL, Japan) and scanning transmission electron microscopy (STEM, Titan G2 60-300, FEI). For the SEM observations, a thin platinum conductive layer was coated on the anodized specimens by a sputter coater (MSP-1S, Vacuum Device, Japan). For the STEM observations, a thin film specimen was obtained through the two steps: the specimen was pasted onto a molybdenum single-hole grid by an epoxy resin and was then thinned by a precision ion polishing system (PIPS, Gatan). The distribution of oxygen and phosphorus in the anodic oxide was examined by STEM-energy dispersive X-ray spectrometry (EDS).

The water contact angles on the aluminum surface anodized via each anodizing condition were measured by an optical contact angle meter (DM-501, Kyowa Interface Science, Japan). For the wettability measurements, the volume of distilled water placed on the surface of the specimens was adjusted to a relatively large amount of 4 μL to evaluate the superhydrophilic behavior in the initial stage of the measurements. The contact angle of the droplet was measured from 100 ms to 2 s just after the water drop was placed on the surface.

3. Results and Discussion

For the formation of various anodic oxides on the aluminum surface, the electropolished aluminum specimens were anodized for t_a = 60 min in the following electrolyte solutions: sulfuric acid, oxalic acid, phosphoric acid, and pyrophosphoric acid. Figure 1a shows a SEM image of the electropolished aluminum surface. Slightly periodic stripe patterns measuring approximately 100 nm in width were observed on the aluminum surface. These stripe patterns were typically formed on the aluminum surface after the electropolishing [38,39]. Figures 1b-1d show SEM images of the aluminum specimens anodized in b) sulfuric acid at 25 V, c) oxalic acid at 50 V, and d) phosphoric acid at 160 V for t_a = 60 min. Many nano- or submicron-scale pores were observed throughout the whole region of the anodic oxide formed via anodizing in these electrolyte solutions. Because constant voltage anodizing was carried out for each electrolyte solution, the diameter of the nanopores that formed in the porous alumina was in the order: sulfuric acid measuring approximately 13 nm < oxalic acid with 33 nm < phosphoric acid with 79 nm. However, it is noted that these values were measured on the porous alumina that was covered by a thin platinum electro-conductive layer for the SEM observations. In contrast, the nanomorphology of the anodic oxide formed by pyrophosphoric acid anodizing at 75 V was considerably different from these porous alumina (Fig. 1e). A honeycomb network nanostructure with thin oxide walls measuring approximately 35 nm in width was distributed across the aluminum surface. In addition, numerous alumina nanofibers were formed at the apices of each honeycomb oxide feature. In our previous study, using transmission electron

microscopy (TEM), these nanofibers were determined to consist of amorphous alumina measuring below 10 nm in diameter [35]. The water contact angle for these nanostructured aluminum surfaces was measured by a contact angle meter for the understanding of surface wettability.

Figure 2 shows the contact angle images of 4-μL water droplets on the electropolished and anodized aluminum surfaces at t_d = 1 s after the water drop was placed on the surface. In this study, the aluminum specimens were used for wettability measurements within 4 h of each anodizing. The bottom black and gray regions correspond to the surface of the specimen, and the hemispherical black parts correspond to the water droplet. The contact angle for the electropolished surface was measured as 30.9°, and a weak hydrophilicity appeared on the electropolished aluminum surface. A thin native oxide film, which is a few nm in thickness, containing a very small amount of chloride ions was formed on the aluminum surface after the electropolishing [40]. This native oxide has a hydrophilic behavior because of the surface-bound hydroxyl (-OH) groups [41,42]. For the porous alumina fabricated via sulfuric, oxalic, and phosphoric acid anodizing (Fig. 2b-2d), the contact angles decreased to 12.4°, 11.3°, and 8.3°, respectively, and superhydrophilicity, a contact angle less than 10°, was achieved with the porous alumina fabricated via phosphoric acid anodizing. The wettability of the porous alumina varies depending on the pore diameter, density, and surface-bound electrolyte molecules used during anodizing. Notably, the contact angle on the anodic oxide formed via pyrophosphoric acid anodizing was a considerably small value of 3.5° (Fig. 2e). It is clear that the aluminum surface covered by anodic alumina nanofibers rapidly exhibited superhydrophilic behavior with a 4-μL-droplet contact angle of less than 5° within 1 s, and the nanofiber-covered surface showed the best hydrophilic property among the anodized specimens examined. It has been reported that the fabrication of “bird’s nest”-like nanostructures are necessary for the superhydrophilic property [43].

Figure 3 shows the time dependence of the water contact angle for the five types of aluminum specimens described in Figs. 1 and 2. The contact angle for the electropolished surface was measured to be 30.5° at t_d = 0.1 s after the water drop was placed, and comparable contact angles were maintained during the measurement until t_d = 2 s. In contrast, the surface of the porous alumina formed via sulfuric, oxalic, and phosphoric acid anodizing exhibited low contact angles measuring 12.2–13.9° at t_d = 0.1 s after the drop was placed. Although these contact angles gradually decreased with time, the decreasing rate of the contact angle became gradual, and nearly steady values were observed in the late stage of the measurements. The contact angle for the aluminum surface anodized in phosphoric acid was lower than that for the surface anodized in sulfuric and oxalic acids for all measurement stages, and a superhydrophilic surface with a contact angle of 6.7° was measured at t_d = 2 s. The contact angle for the surface covered by the alumina nanofibers fabricated via pyrophosphoric acid anodizing exhibited the lowest contact angle of 10.5° immediately after the dropping. Then, the surface is rapidly wetted, and an extremely low water contact angle measuring 2.2° was obtained on the surface at t_d = 2 s. The diameter of the water droplet increased with time after this 2-s-measurement, and this water spreading behavior is described later. It is considered that such excellent wettability generated on the aluminum surface is due to the nanostructural features of the anodic alumina nanofibers in addition to the hydrophilicity of aluminum oxide. Therefore, the effect of the nanomorphology of the anodic alumina formed via pyrophosphoric acid anodizing on the surface wettability was further investigated.

Figure 4a-4c shows SEM images of the specimen anodized in pyrophosphoric acid at 75 V and 293 K for a) t_a = 30 s, b) 4 min, and c) 30 min. After anodizing for 30 s (Fig. 4a), a periodic stripe pattern, which is similar to the electropolished surface, was observed on the aluminum specimen, and it was determined by the SEM observation of the fracture cross-section that the striped pattern was a thin anodic oxide film that formed on the aluminum

substrate (insert figure in Fig. 4a). The shape of the pattern in the anodic oxide then gradually shifts to a porous pattern with anodizing time (Fig. 4b). Interestingly, the fiber-like oxides located at the apices of the bottom of the honeycomb structures were formed via a selective chemical dissolution into the pyrophosphoric acid solution (insert figure in Fig. 4b). Further anodizing causes the formation of long anodic alumina nanofibers on the aluminum specimen because of the growth of alumina layers and the subsequent selective survival of the oxide at the apices (Fig. 4c).

Figure 4d-4f shows a high-angle annular dark field (HAADF)-STEM image and the corresponding oxygen and phosphorus elemental distributions obtained by STEM-EDS analysis. The bottom honeycomb alumina contains phosphorus that is due to the incorporation of anions originating from the electrolyte, which is similar to typical porous alumina. However, it is noted that phosphorus is not found in the apices of the honeycomb alumina structures (see yellow arrows in Fig. 4f), though oxygen is uniformly distributed throughout the oxide. The anodic oxides without anions at each apex remain during long-term pyrophosphoric acid anodizing because of their slow dissolution rate, and numerous anodic alumina nanofibers cover the aluminum surface during anodizing.

Figure 5 shows the time-dependent changes in the contact angle for the specimen anodized in pyrophosphoric acid at 293 K and 75 V for up to t_a = 60 min. As the specimen was anodized for t_a = 30 s, the surface was covered by periodic stripes of the oxide without nanofibers (Fig. 4a) and exhibited a contact angle measuring 10.4° at t_d = 0.1 s after the water drop was placed. The contact angle decreased gradually with time and was measured to be 5.6° at t_d = 2 s after dropping. As the honeycomb oxide and short alumina nanofibers were formed on the surface via anodizing for t_a = 4 min (Fig. 4b), the surface exhibited superhydrophilicity with a contact angle measuring 2.9° at t_d = 2 s after dropping. Further anodizing for t_a = 30 min and 60 min (Figs. 1e and 4c) caused an enhancement of the superhydrophilic behaviors and a contact angle measuring 2.2°. From these contact angle measurements, it is found that the nanofeatures of the anodic oxide in the initial stage of anodizing affected the superhydrophilic behavior of the aluminum surface; to achieve superhydrophilicity, it is important to fabricate the nanofiber-covered aluminum surface. It is noteworthy that we can obtain the superhydrophilic aluminum surface by simple one-step pyrophosphoric acid anodizing for a short time. This excellent superhydrophilicity may be based on the wetting of the water droplet because of the capillary action associated with numerous alumina nanofibers covering the surface.

In a previous study, we reported that low voltage pyrophosphoric acid anodizing caused the formation of high-density anodic alumina nanofibers on the surface, though the growth rate of the nanofibers decreased during anodizing because of the low voltage that was applied [36]. Figure 6a shows SEM images of the aluminum specimen anodized in pyrophosphoric acid at 25 V and 293 K for up to t_a = 60 min. Numerous alumina nanofibers were also fabricated on the surface through the thin barrier and small honeycomb oxide during this low voltage anodizing. However, the density of the nanofibers formed at 25 V was higher than that formed at 75 V and was measured to be approximately 1.1×10^{14} m^{-2} for the latter and 2.7×10^{14} m^{-2} for the former. Figure 6b shows the time-dependent changes in the contact angle on the anodized specimens shown in Fig. 6a. Hydrophilic behaviors similar to those presented in Fig. 5 were measured: 1) the contact angle decreased with time after placing the water drop, and 2) the lowest contact angle was obtained on the surface covered by alumina nanofibers (60 min). However, there was no dependence of the superhydrophilicity on the density of alumina nanofibers, as shown by comparing Fig. 6 with Fig. 5. On the other hand, the achievement of the excellent superhydrophilicity via low voltage anodizing may have an industrial advantage for low-cost fabrication.

Generally, the superhydrophilic property of the material's surface decreases with time in the ambient because of contamination by adsorbed hydrocarbons [44-46]. Figure 7 shows the

changes in the contact angle for a long period of time on the a) electropolished aluminum, b) porous alumina formed via oxalic acid anodizing at 293 K and 50 V for t_a = 60 min, and c) nanofiber-covered surface formed via pyrophosphoric acid anodizing at 293 K and 75 V for t_a = 60 min. In these measurements, the specimens were stored in a desiccator filled with dry air at room temperature, and the contact angles were measured 1 s after the droplet was placed on the surface. The contact angle for the electropolished aluminum surface was measured to be 31.0° after an exposure of t_e = 2 h, and rapidly increased with time until reaching 50.8° because of the contamination by hydrocarbons (Fig. 7a). Conversely, although the contact angles measured on the porous alumina and nanofiber-covered surfaces slightly increased with exposure time, the rates of increase were significantly slower than that of the electropolished aluminum surface. Moreover, the nanofiber-covered surface exhibited and maintained high superhydrophilicity with low contact angles of 4.6°-6.6° during a long-term exposure of t_e = 359 h. The stability and high superhydrophilicity of the aluminum surface covered by alumina nanofibers is important for various industrial applications.

From the wettability measurements, we found that the nanofiber-covered aluminum surface displays a fast and stable superhydrophilic behavior. This novel aluminum surface can be applied to various materials for applications that require highly superhydrophilic properties. Here, we demonstrate two interesting behaviors using the superhydrophilic aluminum surface. Figure 8 shows the surfaces of a) electropolished aluminum surface and b) the aluminum surface anodized with pyrophosphoric acid at 75 V and 293 K for t_a = 1 h after a 10 μL droplet was placed. These aluminum specimens were placed on a hot plate adjusted to 313 K, and then the 10 μL water droplet was placed on the specimens. The environment temperature and humidity during the observation were 295 K and 19.1%, respectively. At t_d = 5 s after dropping (Figure 8a), the water droplet exhibited a hemispherical shape measuring approximately 5.3 mm in diameter on the electropolished aluminum surface, exhibiting a relatively high contact angle. In contrast, the droplet was isotropically spread out on the nanofiber-covered aluminum surface because of its superhydrophilicity. Thereafter, the spreading of the water droplet on the surface continues, and then the water droplet evaporated from the edge of the specimen within t_d = 1 min after dropping (Fig. 8b). Eventually, the surface dried quickly and completely by approximately t_d = 3 min; however, after the same period of time, the large-scale water droplet still remained on the electropolished aluminum surface (Fig. 8d). Such quick-drying aluminum based on the superhydrophilicity of the anodic alumina nanofibers will be useful for various industrial applications, including aluminum plate-fin heat exchangers and pre-sensitized aluminum plate for offset printing.

Figure 9 shows the snow-sliding properties of the electropolished and nanofiber-covered aluminum surfaces. The electropolished aluminum specimen was anodized at 293 K and 75 V for t_a = 60 min, and then the electropolished and anodized aluminum specimens were placed on a rack at a 60° angle to the horizontal and placed outside in the snow. The conditions were -1.4 °C for the ground temperature, 85% humidity, a wind speed of 5.7 m s^{-1}, and 2 cm h^{-1} for the snow accumulation, as measured by the Japan Meteorological Agency in Sapporo. On the electropolished aluminum specimen, many lumps of snow and water droplets adhered to the entire surface (Fig. 9a, left). Conversely, the superhydrophilic aluminum clearly exhibited a mirror-finished surface without snow or water droplets (Fig. 9a, right). Because the superhydrophilic surface can develop a thin water film on the nanofiber-covered surface at approximately zero degrees Celsius, the lumps of snow easily slid to the bottom of the specimen. However, the superhydrophilic surface was covered with snow after a long-term exposure to strong snow (Fig. 9b). The aluminum plate must be slightly heated from the back-side to form the thin water film on the surface for a sustainable slippery aluminum surface, and this can be easily achieved by the high thermal conductivity of aluminum. Such a snow-sliding aluminum combined with a mild heat system will be useful for outdoor materials in regions with heavy

snowfalls.

4. Conclusions

The superhydrophilic behavior of the nanofiber-covered aluminum surface fabricated via pyrophosphoric acid anodizing was investigated. Numerous anodic alumina nanofibers were formed on the aluminum surface through the striped and honeycomb nanostructures. The water contact angle for the nanofiber-covered aluminum decreases with time after a 4-μL drop was placed on the surface, and highly superhydrophilic behavior with a contact angle measuring 2.2° was observed on the surface within 2 s. There was no dependence of the superhydrophilicity on the density of alumina nanofibers fabricated via different constant voltage anodizing conditions. The superhydrophilicity of the nanofiber-covered aluminum is maintained during a long-term exposure test for 359 h. The nanofiber-covered aluminum surface possesses the potential for quick-drying and snow-sliding aluminum materials.

Acknowledgments

This study was conducted at Hokkaido University and was supported by the "Nanotechnology Platform" Program of the Ministry of Education, Culture, Sports, Science, and Technology (MEXT), Japan. The authors would like to thank Mr. Nobuyuki Miyazaki, Mr. Takashi Endo, and Mr. Ryo Oota for their assistance with the SEM and STEM observations. This study was financially supported by the Light Metal Educational Foundation, Japan, the Japan Society for the Promotion of Science (JSPS) "KAKENHI", and Japan Aluminum Association.

Figure captions

Fig. 1 SEM images of the surface of the a) electropolished aluminum specimen and specimens anodized in b) sulfuric acid, c) oxalic acid, d) phosphoric acid, and e) pyrophosphoric acid solutions. The insert figure shows a high magnification image.

Fig. 2 Side views of the 4 μL water droplets on a) the electropolished aluminum surface; the porous alumina formed via b) sulfuric acid, c) oxalic acid, and d) phosphoric acid anodizing; and e) the nanofiber-covered aluminum surface formed via pyrophosphoric acid anodizing. The images were taken t_d = 1 s after the water drop was placed on the surface.

Fig. 3 Change in the water contact angle, θ, as a function of the time, t_d, after the droplet was placed on the electropolished and anodized aluminum surfaces.

Fig. 4 a)-c) SEM images of the surface anodized in pyrophosphoric acid solution at 75 V and 293 K for a) t_a = 30 s, b) 4 min, and c) 30 min. The insert figures show the slide views of each surface. d)-f) HAADF-STEM and elemental distribution mapping images of oxygen and phosphorus in the anodic oxide formed via pyrophosphoric acid anodizing.

Fig. 5 Change in the water contact angle, θ, with the time, t_d, after the droplet was placed on the nanostructured aluminum surfaces formed via pyrophosphoric acid anodizing at 75 V and 293 K for t_a = 30 s – 60 min.

Fig. 6 a) SEM images of the surface anodized in pyrophosphoric acid solution at 25 V and 293 K for t_a = 30 s – 60 min. The insert figures show the slide views of each surface. b) The change in the water contact angle, θ, with the time, t_d, after the droplet was placed on the nanostructured aluminum surfaces described in a).

Fig. 7 Change in the water contact angle, θ, with the exposure time, t_e, for a) the electropolished aluminum and the anodized aluminum formed via b) oxalic and c) pyrophosphoric acid anodizing.

Fig. 8 Photographs of the 10 μL water droplets on the electropolished and nanofiber-covered aluminum specimens for a) t_d = 5 s, b) 1 min, c) 2 min, and d) 3 min 8 s after the droplet was placed. Pyrophosphoric acid anodizing was carried out at 75 V and 293 K for t_a = 1 h.

Fig. 9 Photographs of the surface of the electropolished (left) and nanofiber-covered aluminum (right) specimens in the snow. These specimens were placed on a rack and placed outside in the snow for a) short-time and b) long-time exposure. The conditions were -1.4 °C for the ground temperature, 85% humidity, a wind speed of 5.7 m s^{-1}, and 2 cm h^{-1} for the snow accumulation.

References

[1] G.E. Thompson, Porous anodic alumina: fabrication, characterization and applications, Thin Solid Films 297 (1997) 192–201.
[2] W. Lee, S.-J. Park, Porous anodic aluminum oxide: anodization and templated synthesis of functional nanostructures, Chem. Rev. 114 (2014) 7487–7556.
[3] J.P. O'Sullivan, G.C. Wood, The morphology and mechanism of formation of porous anodic films on aluminium, Proc. Roy. Soc. Lond. A 317 (1970) 511–543.
[4] T. Kondo, H. Miyazaki, K. Nishio, H. Masuda, Surface-enhanced Raman scattering on multilayered nanodot arrays obtained using anodic porous alumina mask, J. Photochem. Photobiol. A 221 (2011) 199–203.
[5] T. Yanagishita, K. Nishio, H. Masuda, Antireflection polymer hole array structures by imprinting using metal molds from anodic porous alumina, Appl. Phys. Express 1 (2008) 067004.
[6] T. Kondo, M. Tanji, K. Nishio, H. Masuda, Cross-striped ordered arrays of Au nanoparticles in anodic porous alumina matrix, Electrochem. Solid-State Lett.9 (2006) C189–C191.
[7] W. Lee, K. Schwirn, M. Steinhart, E. Pippel, R. Scholz, U. Gösele, Structural engineering of nanoporous anodic aluminium oxide by pulse anodization of aluminium, Nat. Nanotechnol. 3 (2008) 234–239.
[8] G.D. Sulka, Highly ordered anodic porous alumina formation by self-organized anodizing, in: A. Eftekhari (Ed.), Nanostructured Materials in Electrochemistry, Wiley-VCH, 2008, pp. 1–116.
[9] G.E. Thompson, G.C. Wood, Porous anodic film formation on aluminium, Nature 290 (1981) 230–232.
[9] T. Kikuchi, T. Yamamoto, R.O. Suzuki, Growth behavior of anodic porous alumina formed in malic acid solution, Appl. Surf. Sci. 284 (2013) 907–913.
[10] T. Kikuchi, O. Nishinaga, S. Natsui, R.O. Suzuki, Fabrication of anodic porous alumina via acetylenedicarboxylic acid anodizing, ECS Electrochem. Lett. 3(2014) C25–C28.
[11] T. Kikuchi, T. Yamamoto, S. Natsui, R.O. Suzuki, Fabrication of anodic porous alumina by squaric acid anodizing, Electrochim. Acta 123 (2014)14–22.
[12] M. Pashchanka, J. J. Schneider, Experimental validation of the novel theory explaining self-organization in porous anodic alumina films. Phys. Chem. Chem. Phys. 15 (2013) 7070-7074.
[12] T. Kikuchi, D. Nakajima, J. Kawashima, S. Natsui, R.O. Suzuki, Fabrication of anodic porous alumina via anodizing in cyclicoxocarbon acids, Appl. Surf. Sci. 313 (2014) 276–285.
[13] D. Nakajima, T. Kikuchi, S. Natsui, R.O. Suzuki, Growth behavior of anodic oxide formed by aluminum anodizing in glutaric and its derivative acid electrolytes, Appl. Surf. Sci. 321 (2014) 364–370.
[14] H. Tsuchiya, S. Berger, J. M. Macak, A. G. Munoz, P. Schmuki, A new route for the formation of self-organized anodic porous alumina in neutral electrolytes, Electrochem. Commun. 9 (2007) 545-550.
[15] S. Akiya, T. Kikuchi, S. Natsui, N. Sakaguchi, R. O. Suzuki, Self-ordered Porous Alumina Fabricated via Phosphonic Acid Anodizing, Electrochimica Acta, 190 (2016) 471-479.
[16] A. Takenaga, T. Kikuchi, S. Natsui, R. O. Suzuki, Self-ordered aluminum anodizing in phosphonoacetic acid and its structural coloration, ECS Solid State Letters, 4 (2015) P55-P58.
[17] A. O. Araoyinbo, M. N. Ahmad Fauzi, S. Sreekantan, and A. Aziz, A novel process to produce nano porous aluminum oxide using alkaline sodium phosphate electrolyte, Asian J. Mater. Sci., 2, 63 (2010).
[18] L. O. Snizhko, A. L. Yerokhin, N. L. Gurevina, D. O. Misnyankin, A. Pilkington, A. Leyland, and A. Matthews, A model for galvanostatic anodising of Al in alkaline solutions, Electrochim. Acta, 50, 5458 (2005).

[19] H. Asoh, K. Nishio, M. Nakao, A. Yokoo, T. Tamamura, H. Masuda, Fabrication of ideally ordered anodic porous alumina with 63 nm hole periodicity usingsulfuric acid, J. Vac. Sci. Technol. B 19 (2001) 569–572.
[20] G.D. Sulka, S. Stroobants, V. Moshchalkov, G. Borghs, J-P. Celis, Synthesis of well-ordered nanopores by anodising aluminium foils in sulphuric acid, J. Electrochem. Soc. 149 (2002) D97–D103.
[21] G.D. Sulka, K.G. Parkoła, Temperature influence on well-ordered nanoporestructures grown by anodization of aluminium in sulphuric acid, Electrochim.Acta 52 (2007) 1880–1888.
[22] L. Zaraska, W.J. Stępniowski, M. Jaskuła, G.D. Sulka, Analysis of nanopore arrangement of porous alumina layers formed by anodizing in oxalic acid atrelatively high temperatures, Appl. Surf. Sci. 305 (2014) 650–657.
[23] G.D. Sulka, W.J. Stępniowski, Structural features of self-organized nanopore arrays formed by anodization of aluminum in oxalic acid at relatively high temperatures, Electrochim. Acta 54 (2009) 3683–3691.
[24] A.P. Li, F. Müller, U. Gösele, Polycrystalline and monocrystalline pore arrays with large interpore distance in anodic alumina, Electrochem. Solid-State Lett.3 (2000) 131–134.
[25] H. Masuda, K. Yada, A. Osaka, Self-ordering of cell configuration of anodic porous alumina with large-size pores in phosphoric acid solution, Jpn. J. Appl. Phys. 37 (1998) L1340–L1342.
[26] Y. Li, Y. Chen, M. Qiu, H. Yu, X. Zhang, X. W. Sun, R. Chen, Preparation of Aluminum Nanomesh Thin Films from an Anodic Aluminum Oxide Template as Transparent Conductive Electrodes, Sci. rep. 6 (2016) 20114.
[27] J. Martín, M. M.-González, J. F. Fernández, O. C. Calero, Ordered three-dimensional interconnected nanoarchitectures in anodic porous alumina, Nature commun. 5 (2014) 5130.
[28] T. Kumeria, M. M. Rahman, A. Santos, J. F.-Borrull, L. F. Marsal, D. Losic, Structural and optical nanoengineering of nanoporous anodic alumina rugate filters for real-time and label-free biosensing applications, Anal. chem., 86 (2014) 1837–1844.
[29] Y. Wang, A. Santos, G. Kaur, A. Evdokiou, D. Losic, Structurally engineering anodic alumina nanotubes as nano-carriers for delivery of anticancer therapeutics, Biomaterials 35 (2014) 5517–5526.
[30] S.Z. Chu, S. Inoue, K. Wada, D. Li, H. Haneda, S. Awatsu, Highly porous (TiO_2-SiO_2-TeO_2)/Al_2O_3/TiO_2composite nanostructures on glass with enhanced photocatalysis fabricated by anodization and sol–gel process, J. Phys. Chem. B 107 (2003) 6586–6589.
[31] N. Q. Zhao, X. X. Jiang, C. S. Shi, J. J. Li, Z. G. Zhao, X. W. Du, Effects of anodizing conditions on anodic alumina structure, J. Mat. Sci. 42 (2007) 3878-3882.
[32] L. A. Meier, A. E. Alvarez, D. R. Salinas, M. C. del Barrio, Formation of dense alumina nanowires from anodic alumina membranes, Mater. Lett. 85 (2012) 146-148.
[33] Y. Kim, S. Lee, H. Cho, B. Park, D. Kim, W. Hwang, Robust superhydrophilic/hydrophobic surface based on self-aggregated Al_2O_3 nanowires by single-step anodization and self-assembly method, ACS Appl. Mat. Inter. 4 (2012) 5074-5078.
[34] Z. L. Xiao, C. Y. Han, U. Welp, H. H. Wang, W. K. Kwok, G. A. Willing, J. M. Hiller, R. E. Cook, D. J. Miller, G. W. Crabtree, Fabrication of alumina nanotubes and nanowires by etching porous alumina membranes, Nano Lett. 2 (2002) 1293-1297.
[35] T. Kikuchi, O. Nishinaga, D. Nakajima, J. Kawashima, S. Natsui, N. Sakaguchi, R.O. Suzuki, Ultla-high density single nanometer-scale anodic alumina nanofibers fabricated by pyrophosphoric acid anodizing, Sci. Rep. 4 (2014)7411.
[36] D. Nakajima, T. Kikuchi, S. Natsui, N. Sakaguchi and R. O. Suzuki, Fabrication of a novel aluminum surface covered by numerous high-aspect-ratio anodic alumina nanofibers, Appl. Surf. Sci., 356 (2015) 54–62.
[37] D. Nakajima, T. Kikuchi, S. Natsui, R.O. Suzuki, Highly ordered anodic alumina

nanofibers fabricated via two distinct anodizing processes, ECS Electrochem. Lett. 4 (2015) H14–H17.
[38] V. V. Konovalov, G. Zangari, R.M. Metzger, Highly ordered nanotopographies on electropolished aluminum single crystals, Chem. Mater. 11 (1999) 1949–1951.
[39] G. Y. Zhao, C. L. Xu, D. J. Guo, H. Li, H. L. Li, Patterning polycrystalline aluminum by electropolishing at low voltages, J. Solid State Electr. 10 (2006) 266-269.
[40] H. Takahashi, M. Nagayama, Surface films formed on aluminum by different pretreatments. I. XPS analysis of thickness and chemical composition, J. Mater. Finish Soc. Jpn. 36 (1985) 96–103.
[41] V. Szczepanski, I. Vlassiouk, S. Smirnov, Stability of silane modifiers on alumina nanoporous membranes, Journal of membrane science 281 (2006) 587-591.
[42] M. Norek, A. Krasiński, Controlling of water wettability by structural and chemical modification of porous anodic alumina (PAA): Towards super-hydrophobic surfaces. Surf. Coat. Tech., 276 (2015) 464-470.
[43] J. Ye, Q. Yin, Y. Zhou, Superhydrophilicity of anodic aluminum oxide films: From “honeycomb” to “bird's nest”. Thin Solid Films, 517 (2009) 6012-6015.
[44] D. Yamamoto, K. Arii, K. Kuroda, R. Ichino, M. Okido, A. Seki, Osteoconductivity of superhydrophilic anodized TiO_2 coatings on Ti treated with hydrothermal processes, J. Biomaterials and Nanobiotechnology 4 (2013) 45–52.
[45] M. Zuldesmi, A. Waki, K. Kuroda, M. Okido, High osteoconductive surface of pure titanium by hydrothermal treatment, J. Biomaterials and Nanobiotechnology 4 (2013) 284–290.
[46] K. Tsougeni, N. Vourdas, A. Tserepi, E. Gogolides, C. Cardinaud, Mechanisms of oxygen plasma nanotexturing of organic polymer surfaces: from stable super hydrophilic to super hydrophobic surfaces. Langmuir, 25 (2009) 11748-11759.

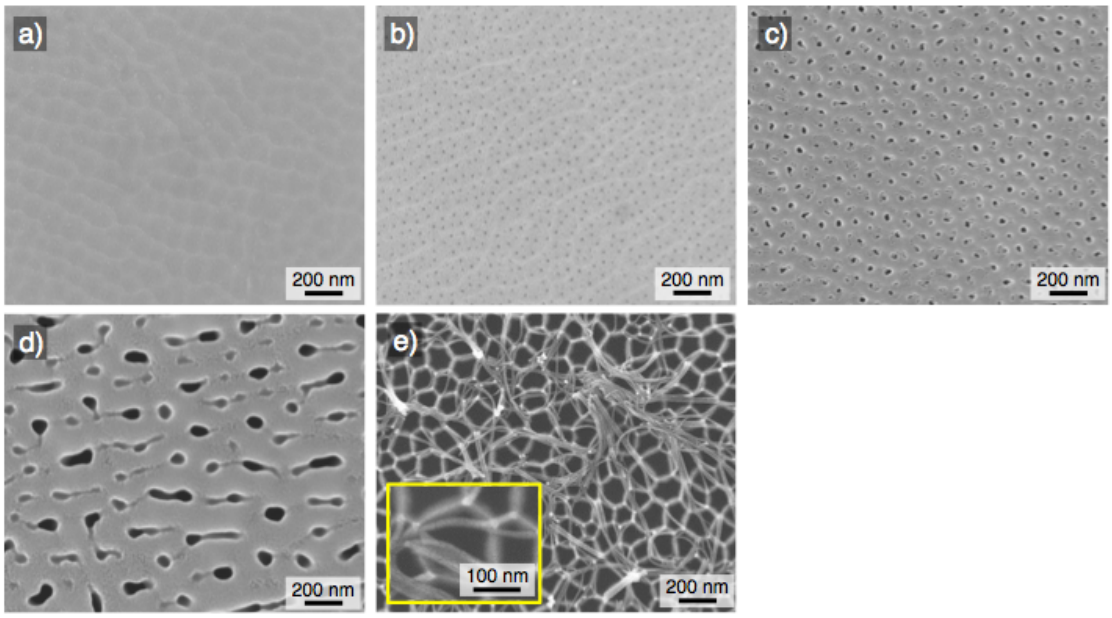

Figure 1

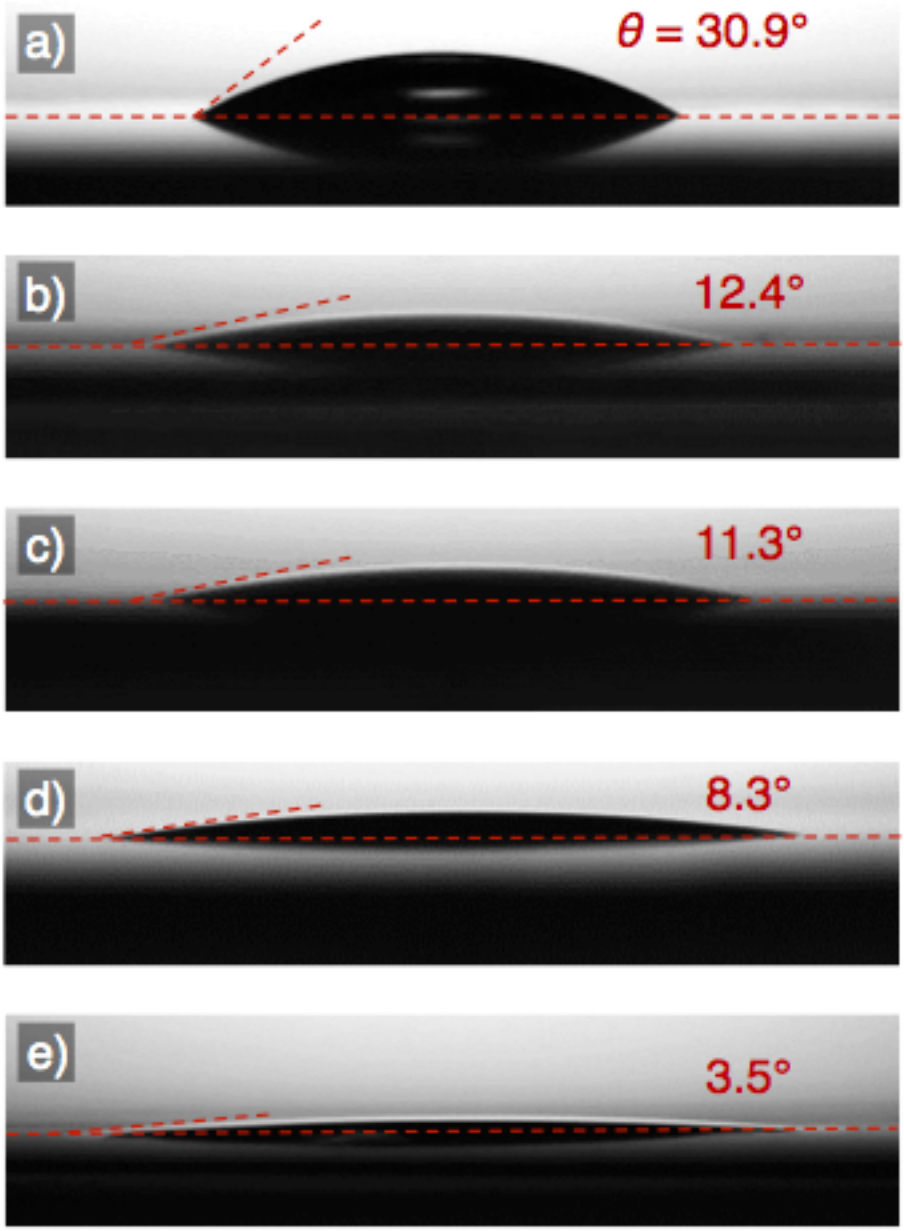

Figure 2

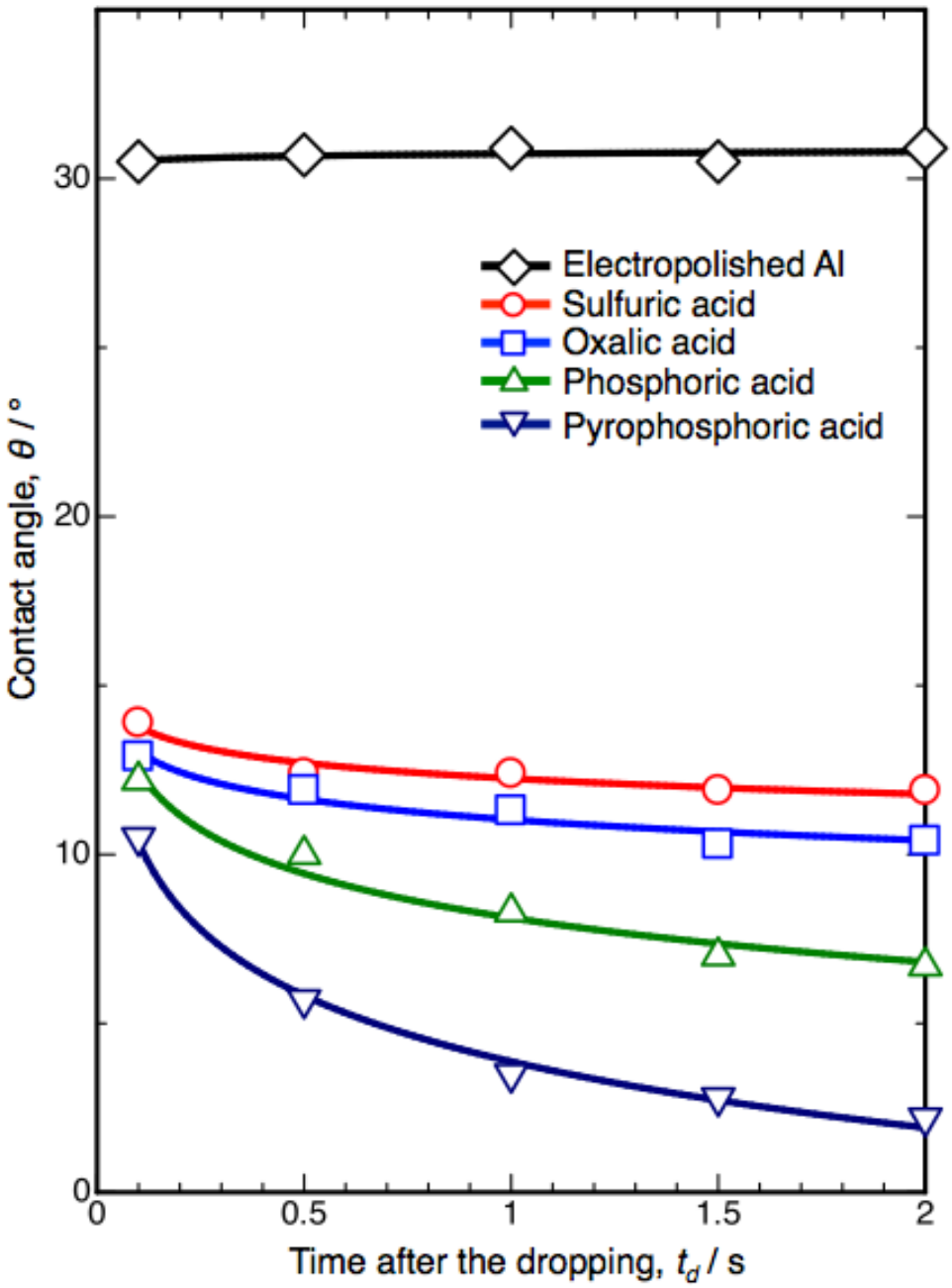
Electropolished Al
Sulfuric acid
Oxalic acid
Phosphoric acid
Pyrophosphoric acid
Contact angle, θ / °
Time after the dropping, t_d / s
0
10
20
30
0
0.5
1
1.5
2

Figure 3

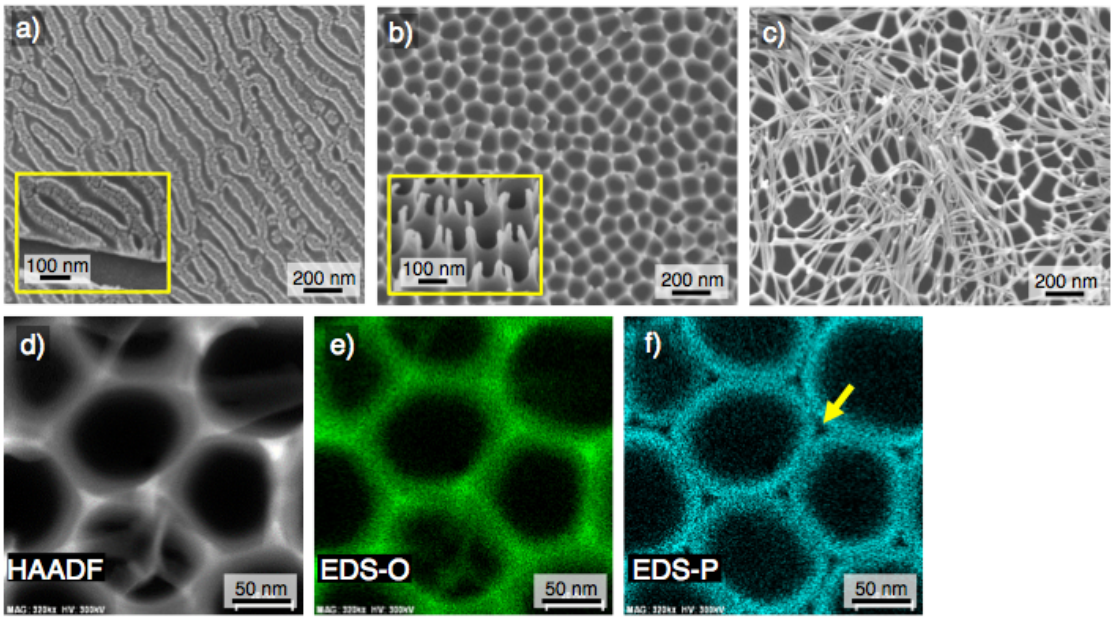
a)
100 nm
200 nm
b)
100 nm
200 nm
c)
200 nm
d)
HAADF
50 nm
e)
EDS-O
50 nm
f)
EDS-P
50 nm

Figure 4

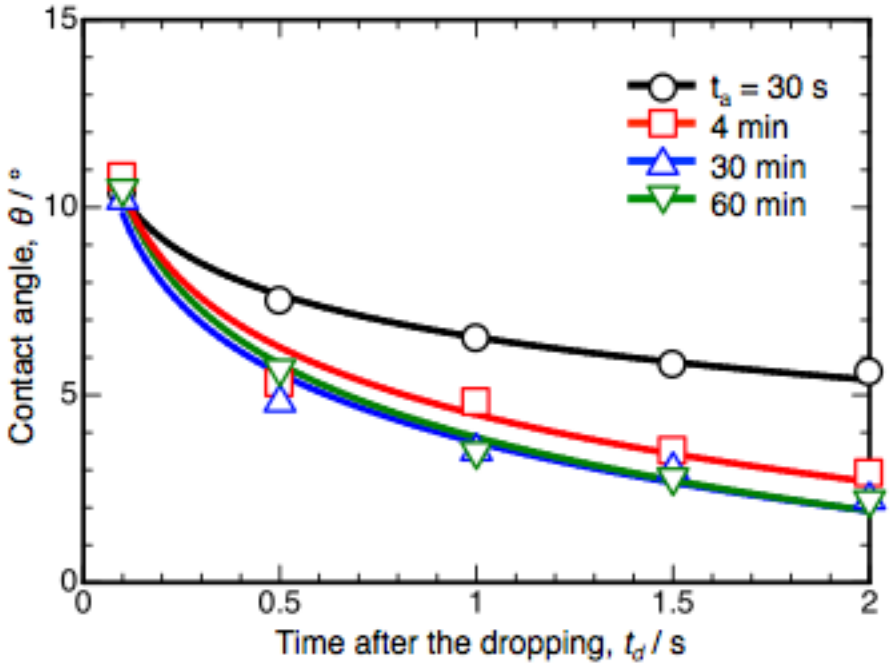
15
10
5
0
0
0.5
1
1.5
2
Contact angle, θ / °
Time after the dropping, t_d / s
t_a = 30 s
4 min
30 min
60 min

Figure 5

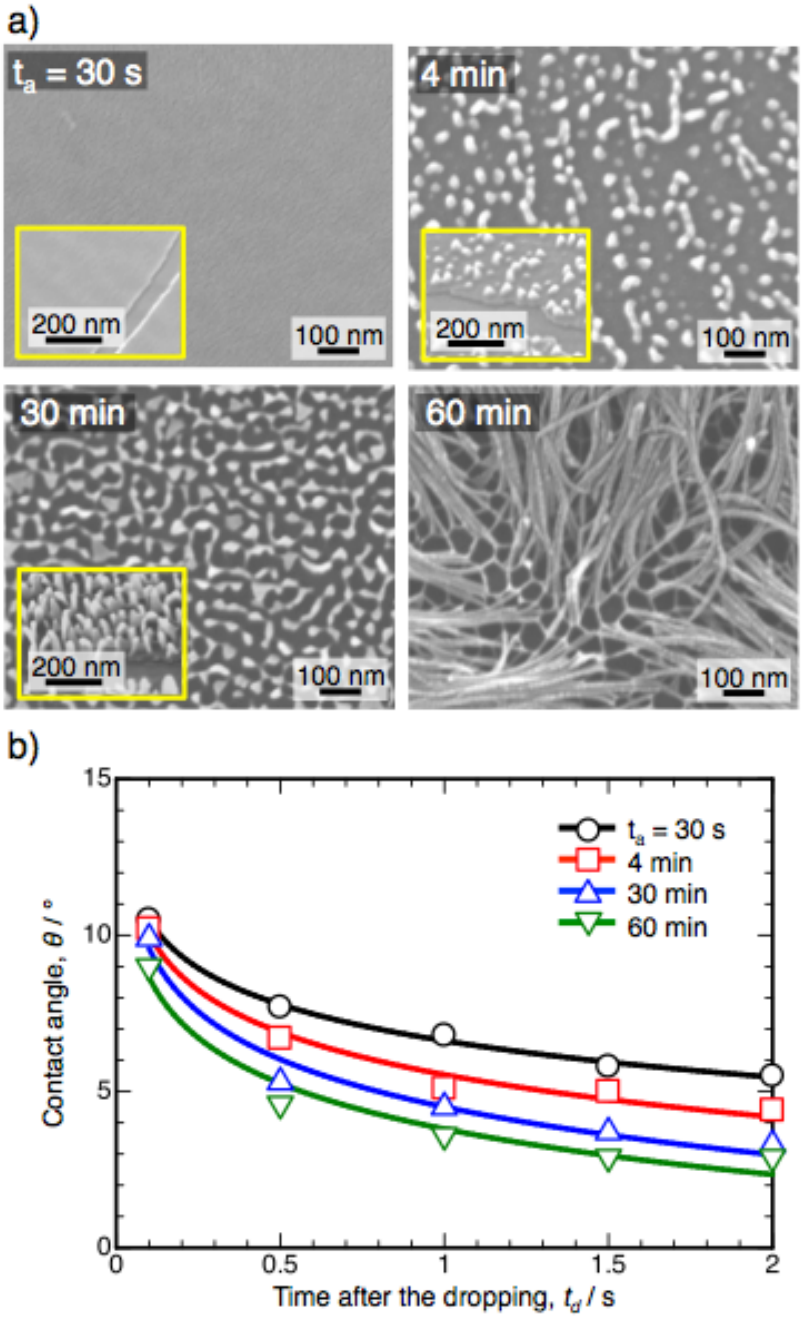
a)
t_a = 30 s
200 nm
100 nm
4 min
200 nm
100 nm
30 min
200 nm
100 nm
60 min
100 nm
b)
15
10
5
0
0
0.5
1
1.5
2
Contact angle, θ / °
Time after the dropping, t_d / s
t_a = 30 s
4 min
30 min
60 min

Figure 6

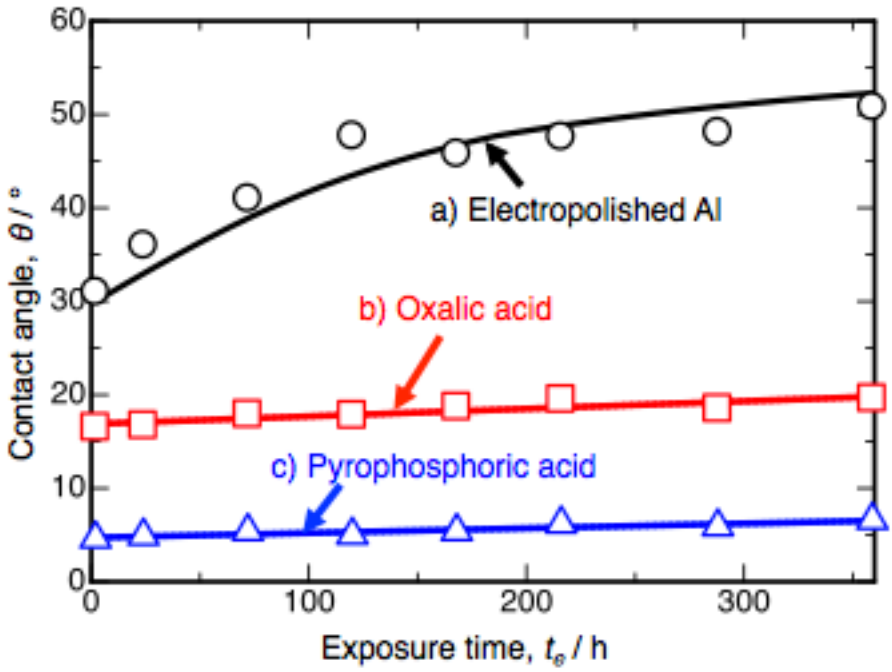
60
50
40
30
20
10
0
0
100
200
300
Contact angle, θ / °
Exposure time, t_e / h
a) Electropolished Al
b) Oxalic acid
c) Pyrophosphoric acid

Figure 7

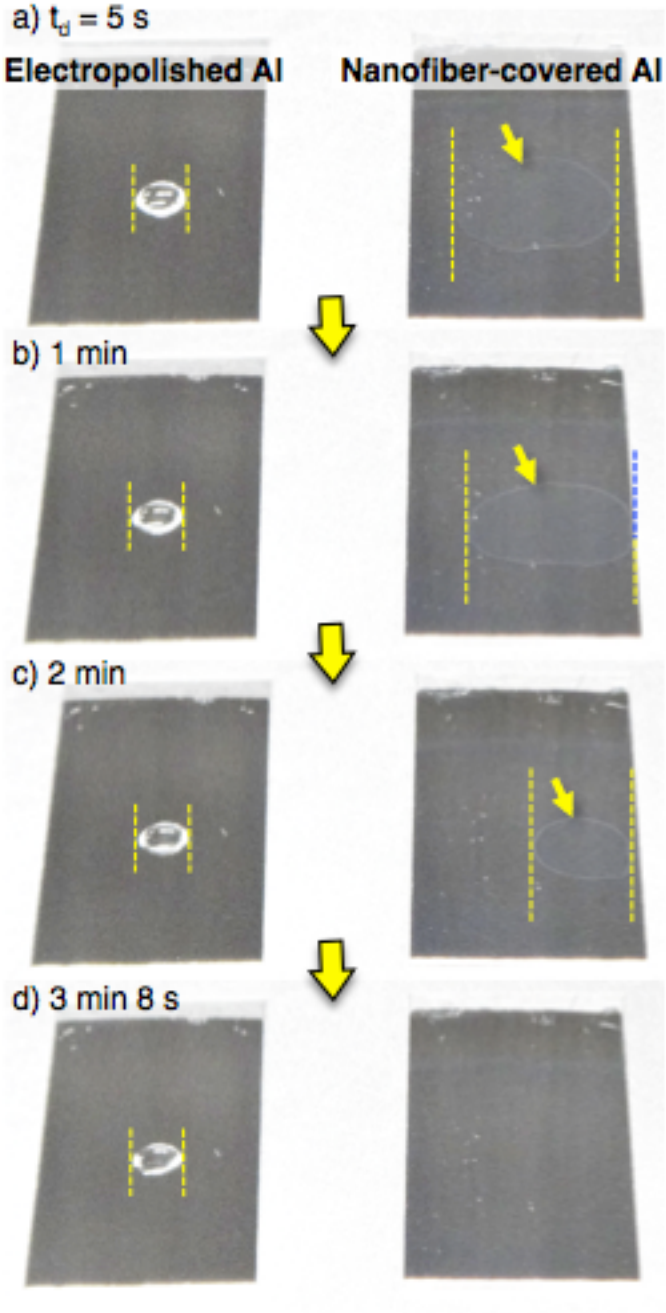
a) t_d = 5 s
Electropolished Al
Nanofiber-covered Al
b) 1 min
c) 2 min
d) 3 min 8 s

Figure 8

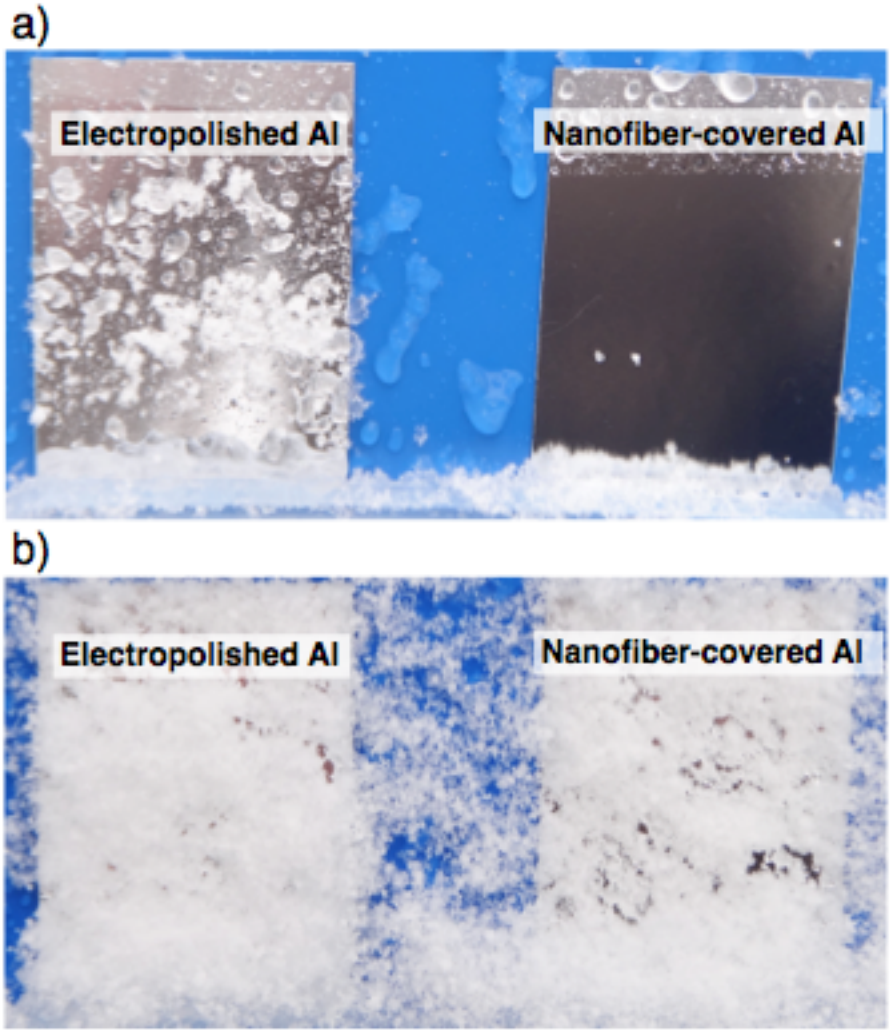
a)
Electropolished Al
Nanofiber-covered Al
b)
Electropolished Al
Nanofiber-covered Al

Figure 9